Performance of the Global Forecast System's Medium-Range Precipitation Forecasts in the Niger River Basin Using Multiple Satellite-Based Products

Haowen Yue[1], Mekonnen Gebremichael[1], and Vahid Nourani[2]

[1] Department of Civil and Environmental Engineering, University of California, Los Angeles, CA 90095-1593
[2] Faculty of Civil Engineering, University of Tabriz, Tabriz, Iran

Correspondence to: Mekonnen Gebremichael (mekonnen@seas.ucla.edu)

Abstract. Accurate weather forecast information has the potential to improve water resources management, energy, and agriculture. This study evaluates the accuracy of medium-range (1 – 15 day) precipitation forecasts from the Global Forecast System (GFS) over watersheds of eight major dams (Selingue Dam, Markala Dam, Goronyo Dam, Bakolori Dam, Kainji Dam, Jebba Dam, Dadin Kowa Dam, and Lagdo Dam) in the Niger river basin using NASA's Integrated Multi-satellitE Retrievals (IMERG) "Final Run" satellite-gauge merged rainfall observations. The results indicate that the accuracy of GFS forecast varies depending on climatic regime, lead time, accumulation timescale, and spatial scale. The GFS forecast has large overestimation bias in the Guinea region of the basin (wet climatic regime), moderate overestimation bias in the Savannah region (moderately wet climatic regime), but has no bias in the Sahel region (dry climate). Averaging the forecasts at coarser spatial scales leads to increased forecast accuracy. For daily rainfall forecasts, the performance of GFS is very low for almost all watersheds except for Markala and Kainji dams, both of which have much larger watershed areas compared to the other watersheds. Averaging the forecasts at longer time scales also leads to increased forecast accuracy. The GFS forecasts, at 15-day accumulation timescale, have better performance, but tend to overestimate high rain rates. Additionally, the performance assessment of two other satellite products was conducted using IMERG Final estimates as reference. The Climate Hazards Group InfraRed Precipitation with Station data (CHIRPS) satellite-gauge merged product has similar rainfall characteristics with IMERG Final, indicating the robustness of IMERG Final. The IMERG "Early Run" satellite-only rainfall product is biased in the dry Sahel region, however in the wet Guinea and Savannah regions, IMERG "Early Run" outperforms GFS in terms of bias. We recommend exploring appropriate post-processing calibration techniques that use near-real time products, such as, IMERG Early, to improve the performance of GFS in the wet regions, particularly at shorter time scales.

1. Introduction

Global climate forecasts, with lead times ranging from hours to several months, are becoming increasingly available (Saha et al. 2014; Abdalla et al. 2013; NCEP 2015; JMA 2019). Significant societal benefit could be realized from research to reduce common barriers in climate forecast utilization blocking the path to improving water resources management, energy, and agriculture. One such a barrier is the lack of understanding of climate forecast accuracy in different regions of the world. This focus is timely given the recent advances in numerical atmospheric models, and in the wealth of new observing capabilities including satellite remote sensing. These combined models and observational datasets provide opportunity for researchers to quantify the accuracy of climate forecasts.

The Niger River is the principal river of West Africa, and is shared among nine riparian countries (Fig. 1): Benin, Burkina Faso, Cameroon, Chad, Guinea, Ivory Coast, Mali, Niger and Nigeria. The basin is facing multiple pressures from increasing population, water abstraction for irrigation, and risk of extreme hydrological events due to climate change (Sylla et al. 2018). A number of hydropower dams exist in the region, and additional dam projects are envisaged in order to alleviate chronic power shortages in the countries of the Niger basin. Optimal management of water resources is key to maximizing benefits, such as hydropower generation, and minimize disasters, such as flooding. Climate forecast information has the potential to improve water resources management, energy, and agriculture (e.g., Patt et al. 2007; Breuer et al. 2010; Mase and Prokopy 2014; Pandya et al. 2015; Koppa et al. 2019; Alexander et al. 2020). For example, in a recent study, Koppa et al (2019) showed that the use of seasonal precipitation forecasts in reservoir planning of Omo Gibe dam in Ethiopia can increase annual hydropower generation by around 40%.

Several studies have investigated the accuracy of seasonal forecasts in West Africa (e.g., Bliefernicht et al. 2019; Pirret et al. 2020). Seasonal forecasts are important for water resource planning, while medium-range (1-day to 15-day) forecasts are important for operational decisions, such as reservoir operations. The availability of medium-range global climate forecasts has grown in recent years. Examples of such forecast products include Global Forecast System (GFS; NCEP 2015), NCEP climate forecast system (NSF CFS, Saha et al. 2014), European Centre for Medium-Range Weather Forecasts (ECMWF; Abdalla et al. 2013), and Global Spectral Model (GSM; JMA 2019). For these precipitation forecasts to be effectively used in applications, their accuracy must be known, which is usually performed
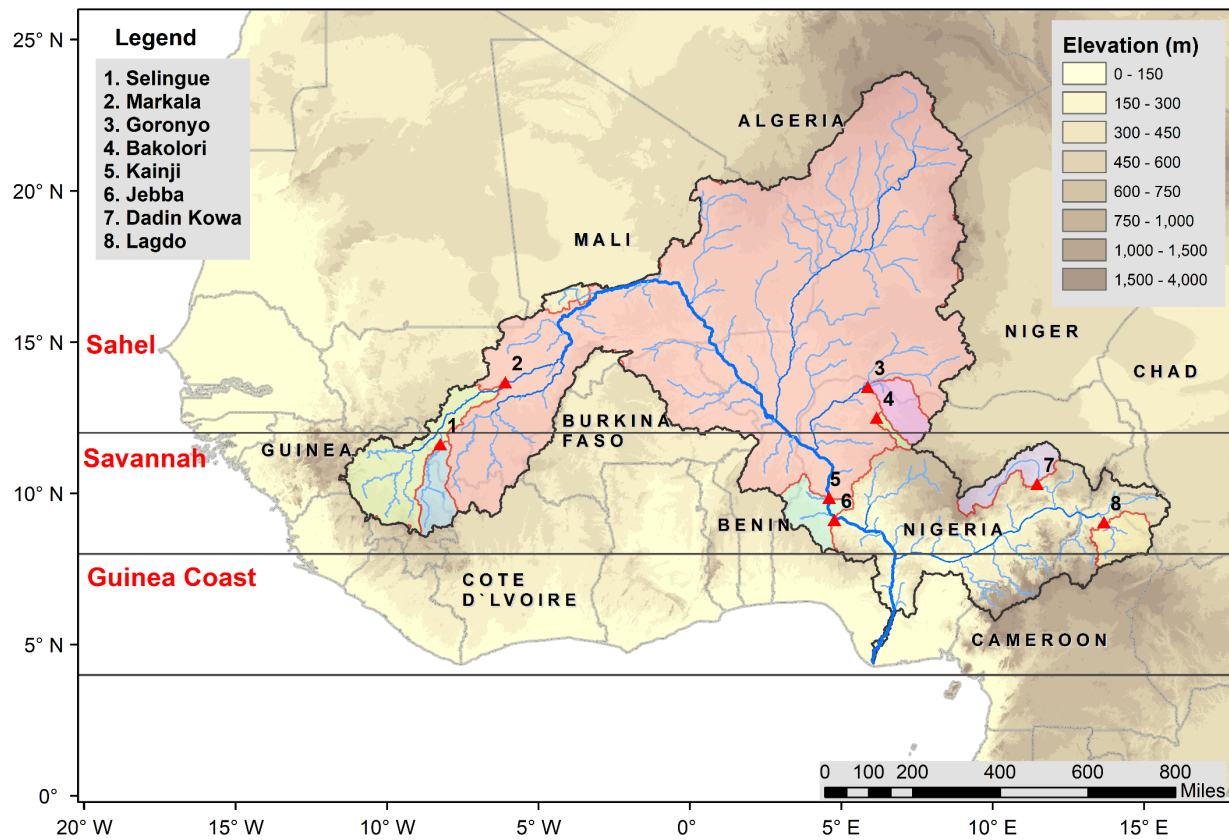
Figure 1. The Niger River Basin, and locations of major reservoir dams in the basin: (1) Selingue, (2) Markala, (3) Goronyo, (4) Bakolori, (5) Kainji, (6) Jebba, (7) Dadin Kowa, and (8) Lagdo.

61   through comparison of precipitation forecasts to observations (e.g., Tian et al. 2017; Yuan et al. 2014). Wang et al.

62   (2019) performed numerical experiment to examine the sensitivity of GFS to inclusion or exclusion of additional

63   observations collected over the eastern Pacific during the El Niño Rapid Response (ENRR) field campaign, type of

64   data assimilation method to prepare the initial conditions, and inclusion or exclusion of stochastic parameterizations

65   in the forecast model. They reported that the GFS forecast errors are only slightly sensitive to the additional ENRR

66   observations, more sensitive to the DA methods, and most sensitive to the inclusion of stochastic parameterizations in

67   the model. In addition, they reported that GFS forecasts have difficulty to capture the location and magnitude of heavy

68   rain rates. Sridevi et al. (2018) evaluated the performance of GFS in India by using rain gauge and satellite rainfall

69   product, and reported that the GFS forecast shows some skills in 1-day and 2-day lead times, but low skills from 3-

70   day onwards. Lien et al. (2016) compared the statistical properties of GFS forecasts and Tropical Rainfall Measuring

71   Mission (TRMM) Multisatellite Precipitation Analysis (TMPA; Huffman et al. 2007, 2010) observations. They

72   reported that the GFS model has positive bias in precipitation amount compared to TMPA observations, and that the

GFS forecasts have large random errors at higher resolutions, especially for convective precipitation. According to Jiang et al. (2015) the lack of consideration of the Aerosol-Cloud Interactions (ACIs) in the GFS model leads to significant bias in the GFS precipitation forecasts.

In our study region of the Niger River basin, there has not been any performance evaluation of GFS precipitation forecasts to date. The Niger basin lies in three different climate regimes (wet regime, moderately wet regime, and dry regime), and is home to nine major irrigation and hydropower dams (Selingue, Markala, Goronyo, Bakolori, Kainji, Jebba, Dadin Kowa, and Lagdo). Recent advances in satellite rainfall products, particularly following the Global Satellite Measurement satellite mission (GPM; Hou et al. 2014), and extensive evaluation of GPM rainfall products in West Africa, provides us with opportunity to use GPM rainfall products as reference for evaluation. Many studies have conducted to evaluate the accuracy of the satellite rainfall estimates in West Africa. Dezfuli et al. (2017a) evaluated the performance of NASA's Integrated Multi-satellitE Retrievals (IMERG) "Final Run" (IMERG Final) (version 4; Huffman et al. 2019a, b) in comparison with two, high-resolution, experimental rain gauge station data provided by the Trans-African Hydro-Meteorological Observatory (TAHMO; van de Giesen et al. 2014), and reported the capability of IMERG Final to represent well the diurnal cycle of rainfall. Using the same dataset, Dezfuli et al. (2017b) showed that IMERG Final is able to capture the propagation of large Mesoscale Convective Systems (MCSs), a significant advantage over its predecessor's (TMPA) 3-hourly temporal resolution, which misses the time evolution of most of these systems. Gossett et al. (2018) evaluated the performance of a number of satellite rainfall products (focusing only on versions that do not include rain gauge data) by comparison with rain gauge station networks in Benin and Niger, and reported that the satellite products (especially IMERG Early) exhibit high performance in Niger but relatively lower performance in Benin. Satgé et al. (2020) evaluated the accuracy of a number of gridded precipitation datasets over West Africa through comparison against rain gauge station data, and reported that CHIRPS and TMPA (the predecessor to IMERG) provided reliable estimates at both daily and monthly timescales, while the remaining satellite products considered (CMORPH, PERSIANN, GSMaP, ARC, and TAMSAT) and all atmospheric reanalysis products considered (MERRA and JRA) were deemed unreliable. Furthermore, they found out that satellite products that incorporated rain gauge information outperformed satellite-only products. Maranan et al. (2020) compared IMERG Final products against experimental rain gauge station data in the moist forest region of Ghana,

100   West Africa, and showed that IMERG Final datasets are able to capture monthly rainfall with a correlation coefficient

101   close to unity.

102

103   The objective of this study is to evaluate the accuracy of medium-range precipitation forecasts derived from the Global

104   Forecast System (GFS) for the major reservoir dams of the Niger basin through comparison against IMERG Final.

105   We chose GFS model due to its relatively high spatial (0.25° x 0.25°) and temporal resolution (3-hourly to 6-hourly)

106   as well as free-of-charge data availability to users. The main questions addressed in this study are as follows. First,

107   how does the accuracy of GFS forecast vary across different reservoir dams in the same basin? Second, how does the

108   accuracy vary with lead time in the range 1- to 15-day? Third, what is the effect of spatial averaging (from 0.25° all

109   the way to basin-scale) and temporal aggregation (from 1-day to 15-day) on the forecast accuracy? Fourth, how does

110   the accuracy of GFS forecast compare with the accuracy of satellite-only rainfall products that are available in near-

111   real-time, as the latter may have the potential to calibrate and improve the accuracy of GFS?

112

113   **2.   Data and Methodology**

114   **2.1 Global Forecast System (GFS) Medium-Range Precipitation Forecasts**

115

116   The Global Forecast System (GFS) is a global numerical weather prediction system run by the U.S. National Weather

117   Service (NWS). The GFS forecast products with a resolution of 0.25° by 0.25° are obtained from National Center for

118   Atmospheric Research (NCAR) Research Data Archive (RDA) GFS Historical Archive (NCEP 2015). The GFS is

119   run four times a day at UTC 00, UTC 06, UTC 12, and UTC 18 hours. One of the GFS model output variables is

120   accumulated precipitation, where the precipitation forecasts are accumulations starting from the model run time. We

121   obtained the 1-day lead daily rainfall forecast by subtracting the 24-hour rainfall accumulation forecast from the 48-

122   hour rainfall accumulation forecast. Similarly, in order to obtain the 5-day lead daily rainfall forecast, we subtracted

123   the 120-hour rainfall accumulation forecast from the 144-hour rainfall forecast. We only considered the model runs at

124   UTC 00 hour.

125

126   The GFS model went through a major upgrade, and its version-15 forecasts are available since June 12, 2019. In

127   version 15, the Finite Volume Cubed Sphere dynamical model (FV3) replaced the Global Spectral Model (GSM) as

128 the core model. In the GSM model, the horizontal resolutions were T1543 (12.5km) from 0 to 240 hours (0-10 days)

129 and T574 (~34km) from 240 to 384 hours (10-16 days) (NCEP 2021a). However, in the FV3 model, the horizontal

130 resolution of the model is about 13 km for days 0-16 (NCEP 2021b). The model runs are re-gridded to produce

131 precipitation forecasts at 0.25° resolution (NCEP 2015). The Key FV3 model schemes include (Putman and Lin 2007):

132 (1) the Rapid Radiative Transfer Method for GCMs (RRTMG) scheme for shortwave/longwave radiation (Mlawer et

133 al. 1997; Iacono et al. 2000; Clough et al. 2005), (2) the Hybrid eddy-diffusivity mass-flux (EDMF) scheme for

134 Planetary Boundary Layer (PBL) (NCEP, 2021a), (3) the Noah Land Surface Model (LSM) scheme for land surface

135 option (Chen et al. 1997), (4) the Simplified Arakawa-Schubert (SAS) deep convection for cumulus parameterization

136 (Arakawa et al. 1974; Grell 1993), and (5) an advanced GFDL microphysics scheme for microphysics (NCEP, 2021b).

137

138 **2.2 IMERG Final Satellite Precipitation Products**

139 IMERG Final rainfall products are used in this study as reference to evaluate the performance of GFS precipitation

140 forecasts. IMERG Final combines all available microwave precipitation estimates, microwave-calibrated infrared

141 estimates, and rain gauge data to provide rainfall estimates at very high resolution (30-minute, 0.10°) (Hou et al. 2014;

142 Huffman et al. 2015). The IMERG products are categorized into three types, namely early run, late run, and final run.

143 It is only the final run or "final" version that incorporates rain gauge data. The data latency of IMERG Final is about

144 3.5 months. Details of IMERG algorithm developed by NASA are available at Huffman et al (2019a, b). The latest

145 version (V6B) of IMERG datasets have been accessed from the NASA's Earth Data Goddard Earth Sciences Data

146 and Information Services Center (GES DISC) web portal.

147

148 **2.3 Other Satellite Precipitation Products**

149 In order to put the GFS forecast performance into perspective, we also evaluated two other state-of-the-art satellite

150 rainfall products:

151 • IMERG Early provides un-calibrated IMERG rainfall fields, which do not include correction from rain gauges.

152 The data latency of IMERG Early is near-real-time, about 4 hours. We have used the latest version (V6B) of

153 IMERG Early datasets. Post-processing calibration of GFS forecasts (in order to improve the accuracy of GFS

154 forecasts) requires the use of "relatively better performing" and "available in near-real-time" independent

155 rainfall observations to correct real-time dynamical GFS model forecasts. Comparison of the performance of

156 IMERG Early with the performance of GFS would indicate to what extent the IMER Early products could be

157 used for calibration of GFS forecasts.

158 • The Climate Hazards Group InfraRed Precipitation with Station data (CHIRPS) is derived primarily from

159 thermal infrared data using the cold cloud duration (CCD) approach, calibrated using TRMM Multi-satellite

160 Precipitation analysis (TMPA 3B42 v7; Huffman et al. 2007) precipitation datasets by local regression, and

161 include rain gauge station data from multiple sources (regional and national meteorological services). CHIRPS

162 data are available at a spatial resolution of 0.05° and a temporal resolution of 1-day, with a data latency period

163 of about 3 weeks. Details of CHIRPS algorithm are available at Funk et al. (2015). Agreement between the

164 reference (IMERG Final) and CHIRPS would indicate that the IMERG Final estimates are robust.

165

166 **2.4 Study Region**

167 The Niger river, with a drainage basin of 2,117,700 Km^2, is the third longest river in Africa. The source of the main

168 river is in the Guinea Highlands, and runs through Mali, Niger, on the border with Benin and then through Nigeria,

169 discharging through a massive delta, known as the Niger Delta (the world's third largest wetland), into the Atlantic

170 Ocean. The rainfall regimes in the region follow the seasonal migration of the Inter-Tropical Convergence Zone

171 (ITCZ), which brings rainfall primarily in the summer season (Animashaun et al. 2020; Sorí et al. 2017).

172 Climatologically, the Niger basin lies in three latitudinal sub-regions (Akinsanola et al. 2015, 2017): (1) the Guinea

173 coast (latitude 4°–8°N), which borders the tropical Atlantic Ocean in the south; (2) the Savannah (latitude 8°–12°N),

174 an intermediate sub-region; and (3) the Sahel (latitude > 12°N) to the north. The Guinea coast experiences a

175 bimodal rainfall regime that is centered in the summer monsoon period of June–September, with August being the

176 period of a short dry season, while the Savannah and Sahel sub-regions experience a unimodal rainfall regime, with

177 maximum rainfall occurring in August (Akinsanola and Zhou 2018). The ranges of annual rainfall amounts are: 400–

178 600 mm in the Sahel, 900–1200 mm in the Savannah; and 1500–2000 mm in the Guinea coast (Akinsanola et al.

179 2017).

180

181 The Niger basin is home to eight major reservoir dams (see Table 1 and Fig. 1): (1) Selingue Dam in Mali: a primarily

182 hydropower dam, (2) Markala Dam in Mali: a primarily irrigation dam, serving about 75,000 ha of farmland, (3)

183 Goronyo Dam in Nigeria: a multi-purpose dam for flood control, provision of downstream water supply and the release

184   of water for irrigation in the dry season, (4) Bakolori Dam in Nigeria: a primarily irrigation dam with a command area

185   of about 23,000 ha, (5) Kainji Dam in Nigeria: the largest Dam on the Niger supplying power for most towns in

186   Nigeria, (6) Jebba Dam in Nigeria: a primarily hydropower dam, (7) Dadin Kowa Dam: a multi-purpose dam for

187   water supply, electricity and irrigation, (8) Lagdo Dam in Cameroon: a multi-purpose dam providing electricity to the

188   northern part of the country and supplying irrigation water for 15,000 hectares of cropland. The watersheds of the

189   dams are primarily either in the Savanna (Selingue, Markala, Jebba, Dadin Kowa, an Lagdo), or in the Sahel (Goronyo,

190   Kainji), or partly in both (Bakolori). The watershed sizes vary over a large range, from 4,887 Km^2 (Bakolori Dam) to

191   1,464,092 Km^2 (Kainji Dam). The average elevations of the watersheds are close to each other at 500 ± 50 m.a.s.l.

192

193   In order to make the results of this study meaningful to reservoir managers, the Niger basin was divided into

194   watersheds according to the locations of the dam reservoirs (see Fig. 1). Then the sub-basin of each dam was defined

195   as the drainage between the dam itself and the upstream dam. For example, the drainage basin of the Markala Dam

196   does not include the drainage basin of the Selingue Dam.

197

198   Table 1. Selected dams and their watershed characteristics

Dam	Country	Operational since*	Capacity (million m³)*	Power (MW)*	Primary Purpose*			Area of Drainage Basin (km²)**	Elevation of Drainage Basin (m)**
					Irrigation and Water Supply	Flood Control	Hydroelectricity		
Selingue	Mali	1982	2170	44			x	32685	473
Markala	Mali	1947	175		x			102882	442
Goronyo	Nigeria	1983	942		x	x		31547	446
Bakolori	Nigeria	1978	450		x			4887	519
Kainji	Nigeria	1968	15000	960			x	1464092	406
Jebba	Nigeria	1984	3600	540			x	40268	308
Dadin Kowa	Nigeria	1988	2855	35	x		x	32936	535
Lagdo	Cameroon	1983	7800	72		x	x	31352	452

199 * information obtained from the Global Reservoir and Dam Database (Lehner et al. 2011) and Food and Agriculture Organization
200 of the United Nations (FAO)'s Global Information System on Water and Agriculture (AQUASTAT).
201 ** Calculated from HydroSEHDS (Lehner et al. 2008).
202
203
204   **2.5 Evaluation**

205   IMERG Final rainfall products are used in this study as reference to evaluate the performance of GFS precipitation

206   forecasts. The comparison period is 15 June 2019 to 15 June 2020 to match the period for which the version-15 of

For evaluation metrics, we used the modified Kling-Gupta Efficiency (KGE; Gupta et al. 2009; Kling et al. 2012) and its components: Bias Ratio (BR), correlation (R), and variability ratio (γ). *KGE* measures the goodness-of-fit between estimates of precipitation forecasts and reference observations as:

$$KGE = 1 - \sqrt{(R-1)^2 + (BR-1)^2 + (\gamma-1)^2},$$

$$BR = \frac{\mu_f}{\mu_o},$$

$$\gamma = \frac{CV_f}{CV_o},$$

where R is the linear correlation coefficient between forecasted and observed precipitation, BR is the bias ratio, γ is the variability ratio, μ is the mean precipitation, CV is the coefficient of variation, and the indices *f* and *o* represent forecasted and observed precipitation values, respectively. KGE values range from -∞ to 1, with values closer to 1 indicating better model performance. Towner et al. (2019) suggested the following classifications: "Good" (KGE ≥ 0.75), "Intermediate" (0.75 ≥ KGE ≥ 0.5), "Poor" (0.5 ≥ KGE > 0), and "Very poor" (KGE ≤ 0). The *BR* values greater than 1 indicate a positive bias whereby forecasts overestimate precipitation relative to the observed data, while values less than 1 represent an underestimation. *The γ* values greater than 1 indicate that the variability in the forecast time series is higher than that observed, and values less than 1 show the opposite effect. The *R* measures the strength and direction of the linear relationship between the forecast and observed values, and to what extent the temporal dynamics of observed rainfall is captured in the forecasts. The correlation values of 0.6 or more are considered to be skillful (e.g., Alfieri et al. 2013). In addition, the root mean-square-error normalized by reference precipitation mean (NRMSE) was also used.

3.   Results and Discussion

3.1 Annual Spatial Variability and Seasonal Characteristics

The spatial map of annual (15 June 2019 – 15 June 2020) rainfall from the various rainfall products is given in Figure 2. According to the reference rainfall product (i.e. IMERG Final), the Niger basin experiences average annual rainfall of 700 mm. The spatial rainfall distribution shows north-to-south increasing gradient, with the Sahel region (> 12°N) receiving on average 346 mm per year, the Savanna region (8°N – 12°N) receiving on average 1,206 mm per year, and the Guinea region (4°N – 8°N) receiving on average 1,620 mm per year. The spatial structures (climatology and north-south gradient in rainfall) of GFS, IMERG and CHIRPS rainfall fields are quite similar to those of IMERG Final. However, the 1-day GFS tends to overestimate in the wet Guinea region of the basin, whereas both IMERG Early and CHIRPS give values that are very close to IMERG Final.
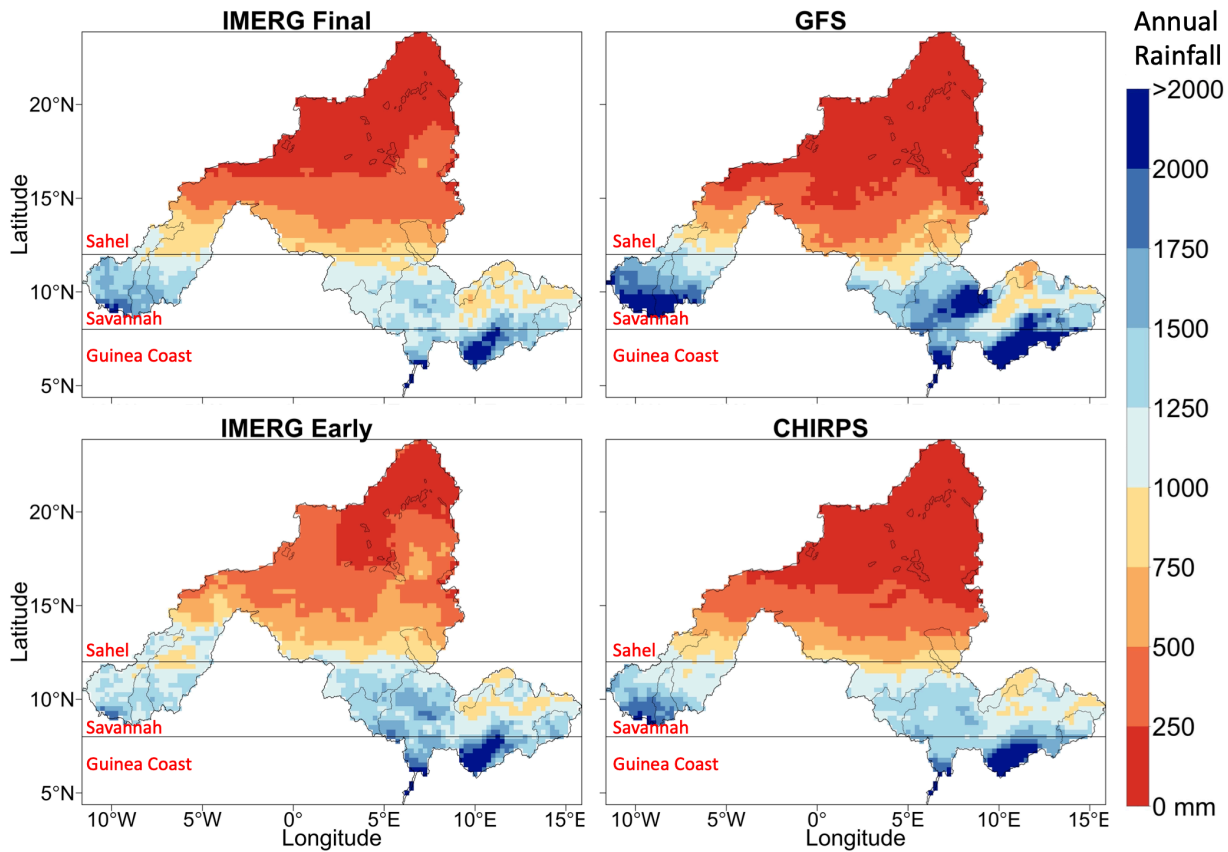
Figure 2. Spatial map of annual rainfall (in mm), for the period 15 June 2019 to 15 June 2020, derived from (a) IMERG Final, (b) GFS (1-day lead time), (c) IMERG Early, and (d) CHIRPS.

247   Figure 3 shows the seasonal rainfall pattern for each climatological region. According to the reference IMERG Final,

248   as one goes from north to south, the rainy season expands from 3 months (June – September) in the Sahel to 6 months

249   (March – November) in the Savanna and Guinea regions. The peak rainfall also shows north-south gradient, with peak

250   rainfall of 130 mm in the Sahel, to 269 mm in the Savanna, and 350 mm in the Guinea. The rainfall pattern is unimodal

251   with a peak rainfall value in August for both Sahel and Savanna, but becomes bimodal with one peak in May and the

252   other in September for Guinea.

253
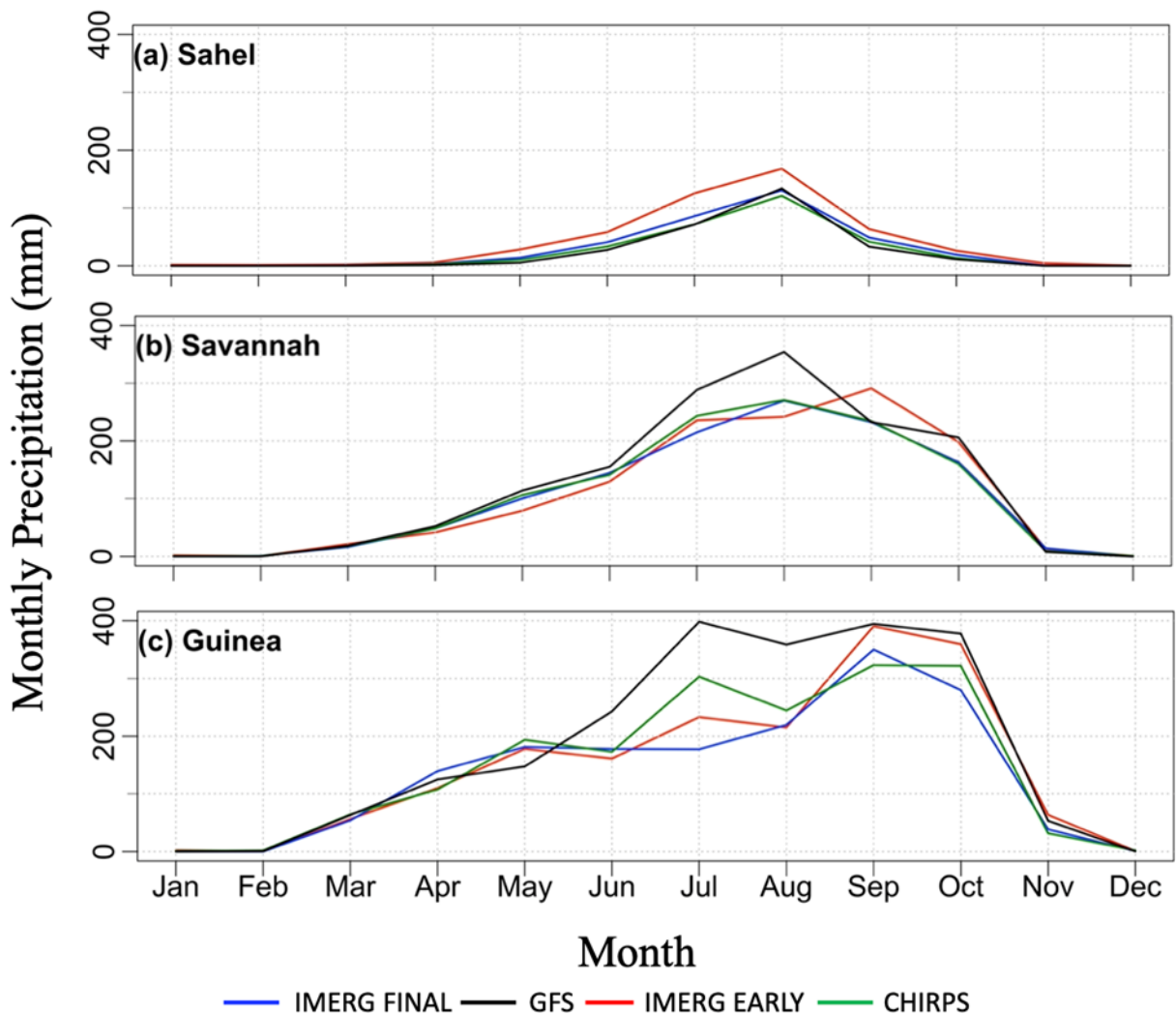
254   Figure 3. Monthly precipitation regime for the three climatological zones of the Niger river Basin: (a)
       Sahel, (b) Savanna, and (c) Guinea. Analyses are based on rainfall fields derived from IMERG Final, 1-
255   day-lead GFS. IMERG Early, and CHIRPS. The time period covers from 15 June 2019 to 15 June 2020.

256

257 When validated against IMERG Final, the performance of GFS in capturing the seasonal rainfall characteristics

258 deteriorates as one goes from north to south. GFS captures both the seasonal rainfall pattern and rainfall peak in the

259 Sahel, and captures the seasonal rainfall pattern but tends to moderately overestimate the peak in the Savannah, while

260 it has large overestimation (almost twice as much as the reference) in the Guinea particularly during summer. As far

261 as the other satellite products are concerned, IMERG Early tends to slightly overestimate in the Sahel across all rainy

262 months, but performs relatively well in the Savannah and Guinea regions. CHIRPS is very close to IMERG Final in

263 all regions and months, with the exception of modest overestimation of the July rainfall in Guinea.

264

265 **3.2 How well do GFS forecasts capture annual rainfall?**

266 Here, we aggregate the 1-day lead GFS forecasts to annual time scale and compare the results against corresponding

267 annual precipitation estimates from IMERG Final. Figure 4 presents the watershed-averaged annual rainfall for each

268 dam watershed. According to IMERG Final, the annual rainfall varies from 434 mm (in Kainji) to 1,481 mm (in

269 Selingue). Watersheds 1 (Selingue) and 2 (Markala), located in the western part of the Savannah, receive the largest

270 amount of rainfall, i.e., 1481 mm and 1406 mm, respectively. Watershed 3 (Markala), located in the eastern part of

271 the Sahel, receives 741 mm of annual rainfall. Watershed 4 (Bakolori), characterized by the smallest watershed area

272 compared to the rest of the watersheds, lies partly in the Sahel and partly in the Savannah region and receives 921 mm

273 of annual rainfall. Watershed 5 (Kainji), characterized by the largest watershed area of all, lies mostly in the Sahel

274 region and receives the lowest amount of annual rainfall (434 mm). Watersheds 6 (Jebba), 7 (Dadin Kowa), and 8

275 (Lagdo), located in the Savannah, receive annual rainfall amounts of 1190 mm, 941 mm, and 1295 mm, respectively.

276

277 Validated against IMERG Final, the GFS tends to overestimate rainfall in all watersheds located in the Savannah (or

278 watersheds that receive relatively large rainfall amounts), with an overestimation varying in the range 8% to 33%,

279 with larger bias for watersheds receiving higher rainfall amount. For watersheds in the Sahel (watersheds receiving

280 low rainfall amount), GFS gives less bias (-11% for the driest Kainji watershed and +10% for Bakolori).

281

282 In contrast, IMERG Early tends to underestimate rainfall in all watersheds located in the Savannah (with larger

283 negative bias in watersheds with large rainfall amount) but tends to overestimate in all watersheds located in the Sahel

284 (with very large overestimation bias for the driest watershed) Therefore, GFS and IMERG Early have different bias

characteristics: whereas GFS outperforms IMERG Early in the Sahelian climate where well-organized convective systems dominate the monsoon, IMERG Early outperforms GFS in the Savannah and Guinea climate which are characterized by short-lasting and localized systems and wet land surface conditions. CHIRPS estimates are reasonably close to IMERG Final, indicating that the choice of reference product between CHIRPS and IMERG Final would not substantially affect the findings on the accuracy of GFS forecasts.
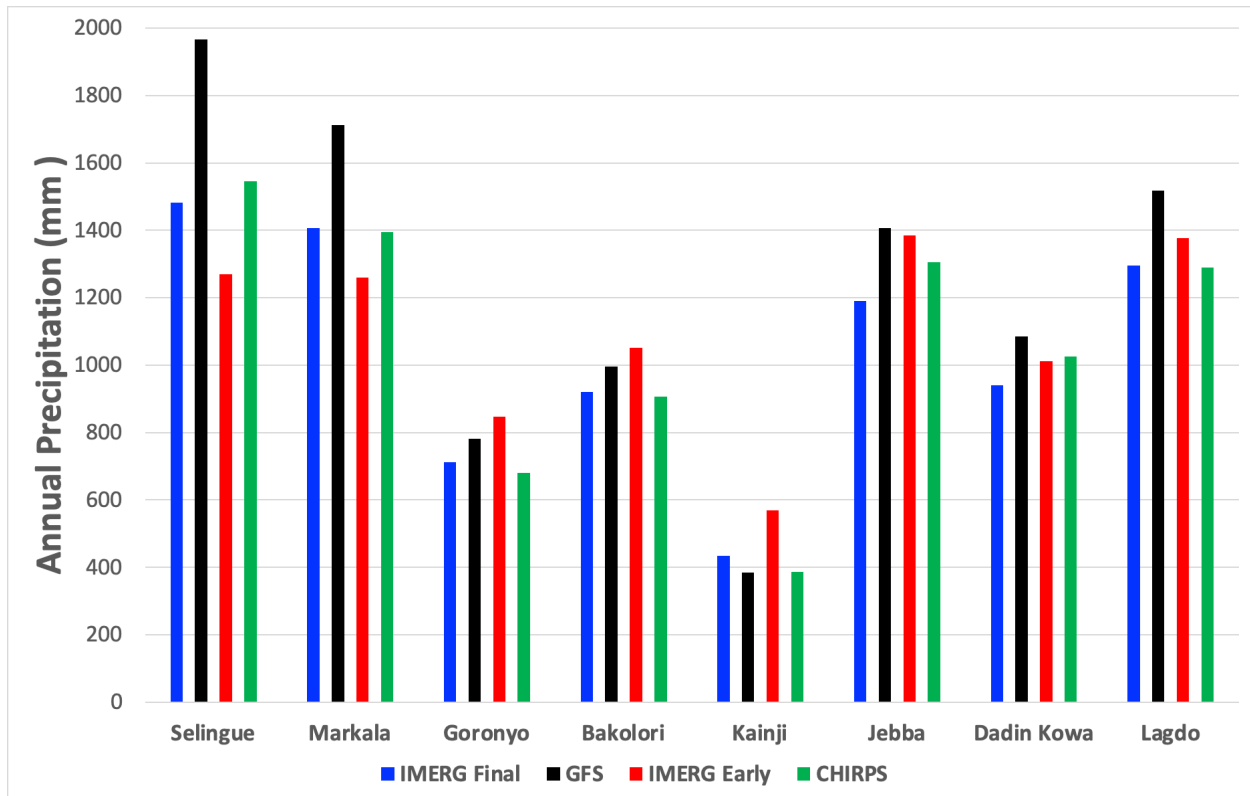
Figure 4. Sub-basin averaged annual precipitation (mm) for the period, 15 June 2019 to 15 June 2020, for each of the Niger's sub-basin, derived from the 1-day lead GFS forecast and different satellite precipitation products.

3.3 How well is the time series of daily precipitation forecasted?

Figures 5 and 6 present the time series of watershed-averaged daily rainfall, for the wet period June – October. According to IMERG Final, the temporal variability (as measured through coefficient of variation or CV) varies from 1.22 to 2.60. Validated against IMERG Final, the GFS tends to underestimate the temporal variability and particularly underestimate large spikes in rainfall, at almost all sites except at Kainji. The GFS's relatively better performance for

300   Kainji could be attributed to the watershed's large area that results in relatively smooth temporal variability. Both

301   IMERG Early and CHIRPS provide CV values that are very close to IMERG Final.
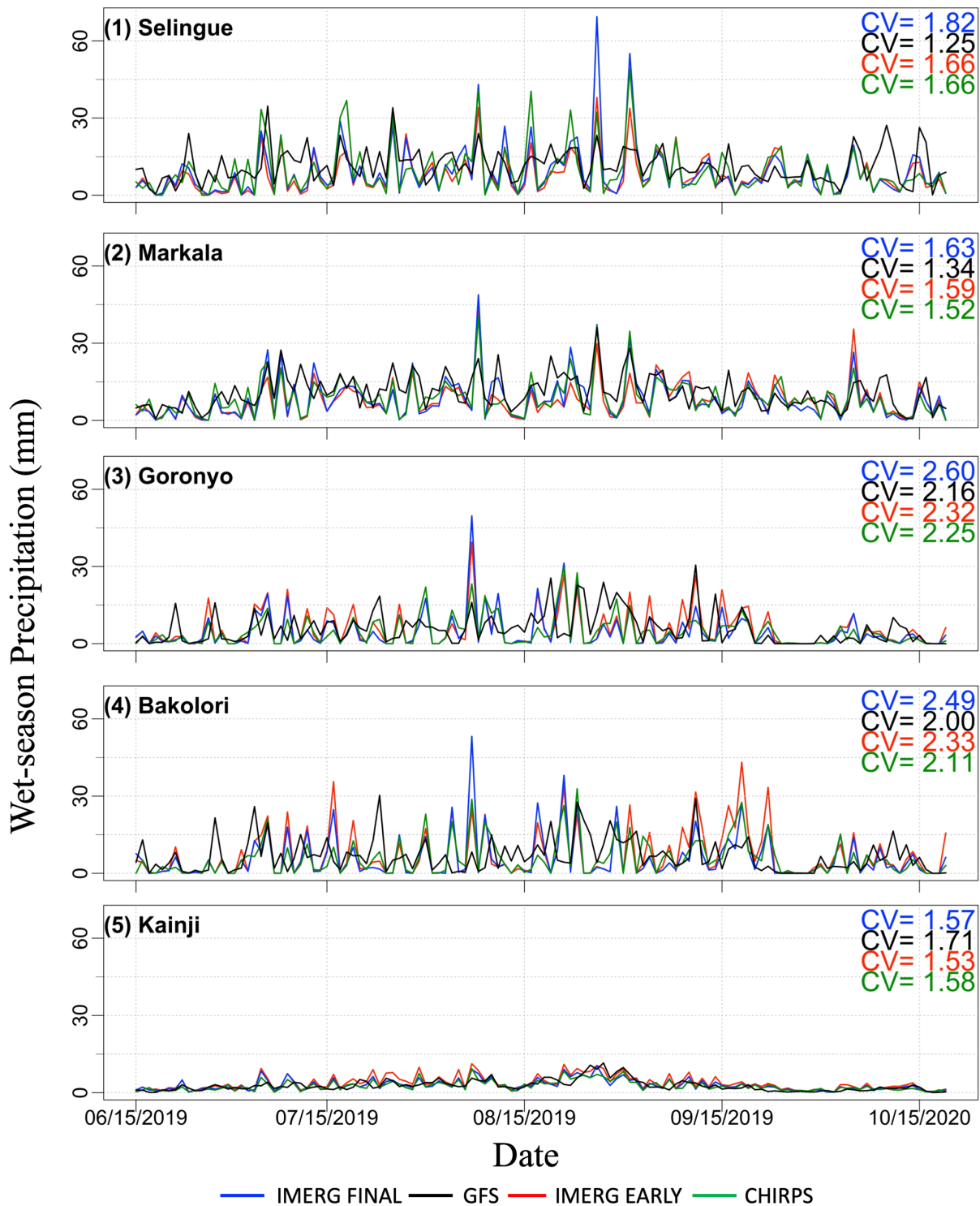
302   Figure 5. Time series of sub-basin averaged precipitation total (mm) for the wet period (June – September 2019 for
303   all sub-basins, derived from various precipitation products, for five sub-basins. The Figure also shows the
304   coefficient of variation (CV) as a measure of temporal variation.
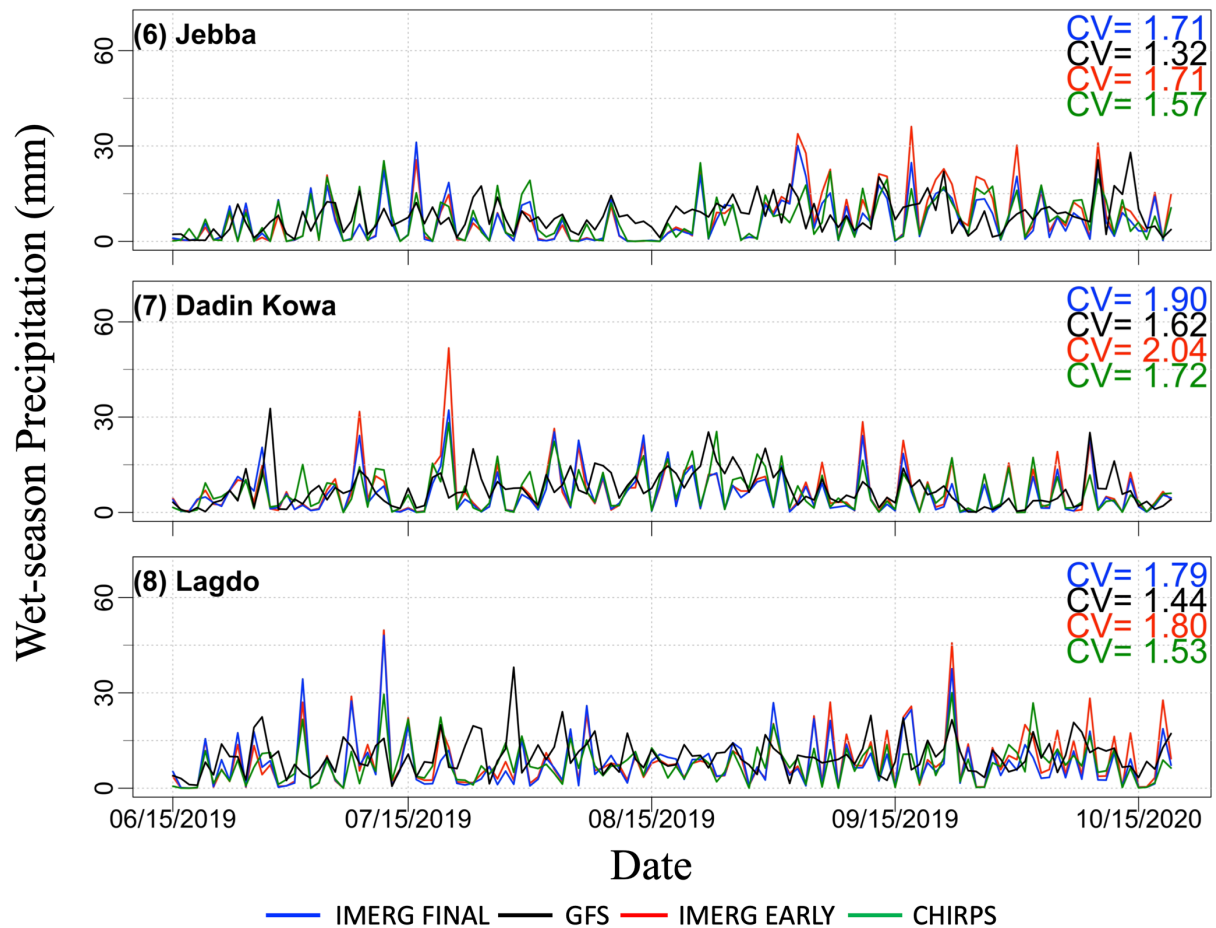
Figure 6. Same as in Figure 5 but for the remaining three watersheds.

Figure 7 displays the performance statistics of watershed-averaged daily rainfall (validated against IMERG Final) in terms of Kling-Gupta Efficiency (KGE), Bias Ratio (BR), correlation (R), variability ratio (γ), and root mean square error normalized by reference precipitation mean (NRMSE). First, the performance results for the 1-day lead GFS are considered. The KGE scores are poor ($0.3 <$ KGE < 0.5) for half of the watersheds considered (Selingue, Goronyo, Bakolori, and Lagdo) and intermediate ($0.5 <$ KGE < 0.75) for the remaining half watersheds (Markala, Kainji, Jebba, and Dadin Kowa). The breakdown of the KGE scores (BR, R, and γ) reveals the key factors contributing to the KGE estimates. The GFS tends to overestimate daily precipitation for most sub-basins, as BR is higher than one, except for Kainji. The overestimation is particularly high for Selingue and Markala, where BR is 1.33 and 1.22, respectively. The correlation coefficient between GFS and IMERG Final is mostly low ($R < 0.60$), and is particularly lower for Bakolori (R=0.36) and Goronyo (R=0.43). The variability ratio of GFS is mostly between 0.69 to 0.83 (except for

317   Kainji, where γ is 1.09), indicating that the GFS tends to give lower temporal variability of rainfall. The NRMSE is

318   very high, ranging from 100% to 266%, and is particularly high for Goronyo (266%) and Bakolori (264%), which are

319   relatively small-sized watersheds.

320

321   Next, the performance of IMERG Early was examined with respect to IMERG Final, mainly to assess if it is possible

322   to use the near-real-time IMERG Early product to calibrate and improve the accuracy of GFS forecasts. The IMERG

323   Early performs much better with KGE values higher than 0.75 (except for Kainji where KGE is 0.69), correlation

324   higher than 0.90, and variability ratio close to the optimum value. The high performance of IMERG Early is due to its

325   similarity with the IMERG Final product, as the main difference between the two products is that IMERG Early,

326   unlike IMERG Final, does not use monthly rain gauge observations for bias correction. Such monthly bias correction

327   techniques would not alter the pattern and variability of IMERG Early compared to IMERG Final. Therefore, the

328   performance of IMERG Early should be evaluated using bias statistics, the other statistics (correlation and variability

329   ratio) are presented for completeness. IMERG Early overestimates rainfall in most watersheds in the range 11%

330   (Lagdo) to 28% (Kainji) except for two watersheds, where it slightly underestimates by 14% (Selingue) and 11%

331   (Markala). Comparison of the performance of GFS and IMERG Early indicates that both products have different bias

332   characteristics. In some watersheds (e.g., Kainji), GFS outperforms IMERG Early in terms of bias, whereas in other

333   watersheds (e.g., Markala), IMERG Early outperforms GFS.

334

335   CHIRPS was also compared with IMERG Final to assess how the use of different reference products may affect the

336   finding about the performance of GFS forecasts. The KGE scores of CHIRPS are higher than 0.75 in all cases,

337   indicating that CHIRPS and IMERG Final have comparable KGE performance. Therefore, the performance of GFS

338   is expected to be about the same even if the reference product used this in this study (IMERG Final) changes to

339   CHIRPS.

340

341

342

343

344
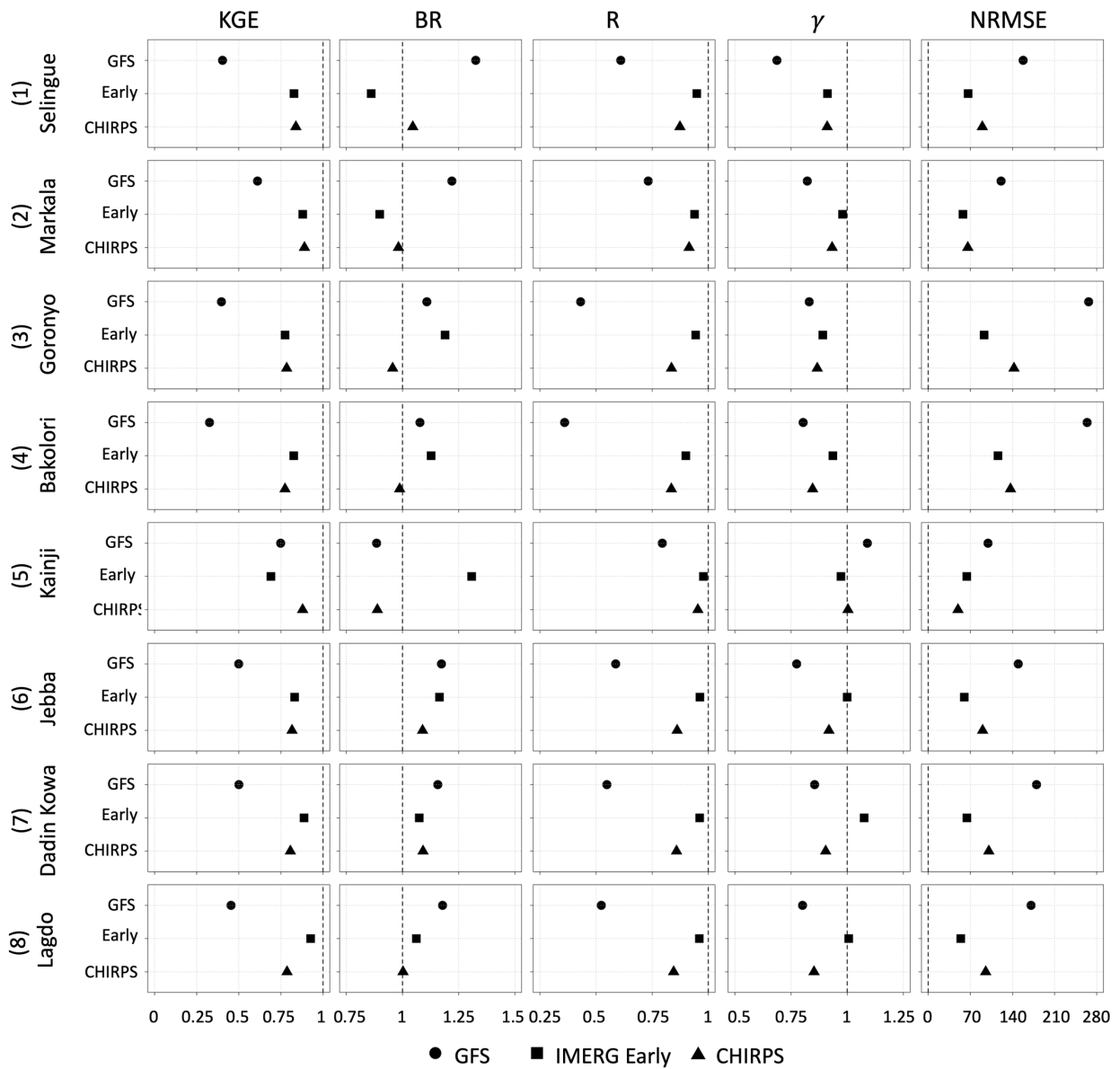
347 Figure 7. Summary of performance statistics (Kling-Gupta Efficiency KGE, Bias Ratio BR, correlation R,
348 variability ratio γ, and root mean square error normalized by reference rainfall [%], for the 1-day lead time GFS
349 forecasts and other satellite products. The time period considered was June 15, 2019 – June 15, 2020.
350

3.4 Dependence of Forecast Performance on Precipitation Rate

352 Figure 8 presents the scatterplot of 1-day lead GFS forecasts and IMERG Final at daily and watershed-average scales.

353 The performance of GFS varies between watersheds. In the Markala and Kainji watersheds, GFS forecasts agree well

354 with IMERG Final at almost all rain rates. In the Selingue watershed, GFS agrees well with IMERG Final for rain

355 rates under 30 mm/day, but GFS substantially underestimates all rain rates above 30 mm/day. In the remaining five

356 watersheds, GFS has poor performance, replete with large scatter, high false alarm, and large underestimation bias of

357 heavy rain rates.
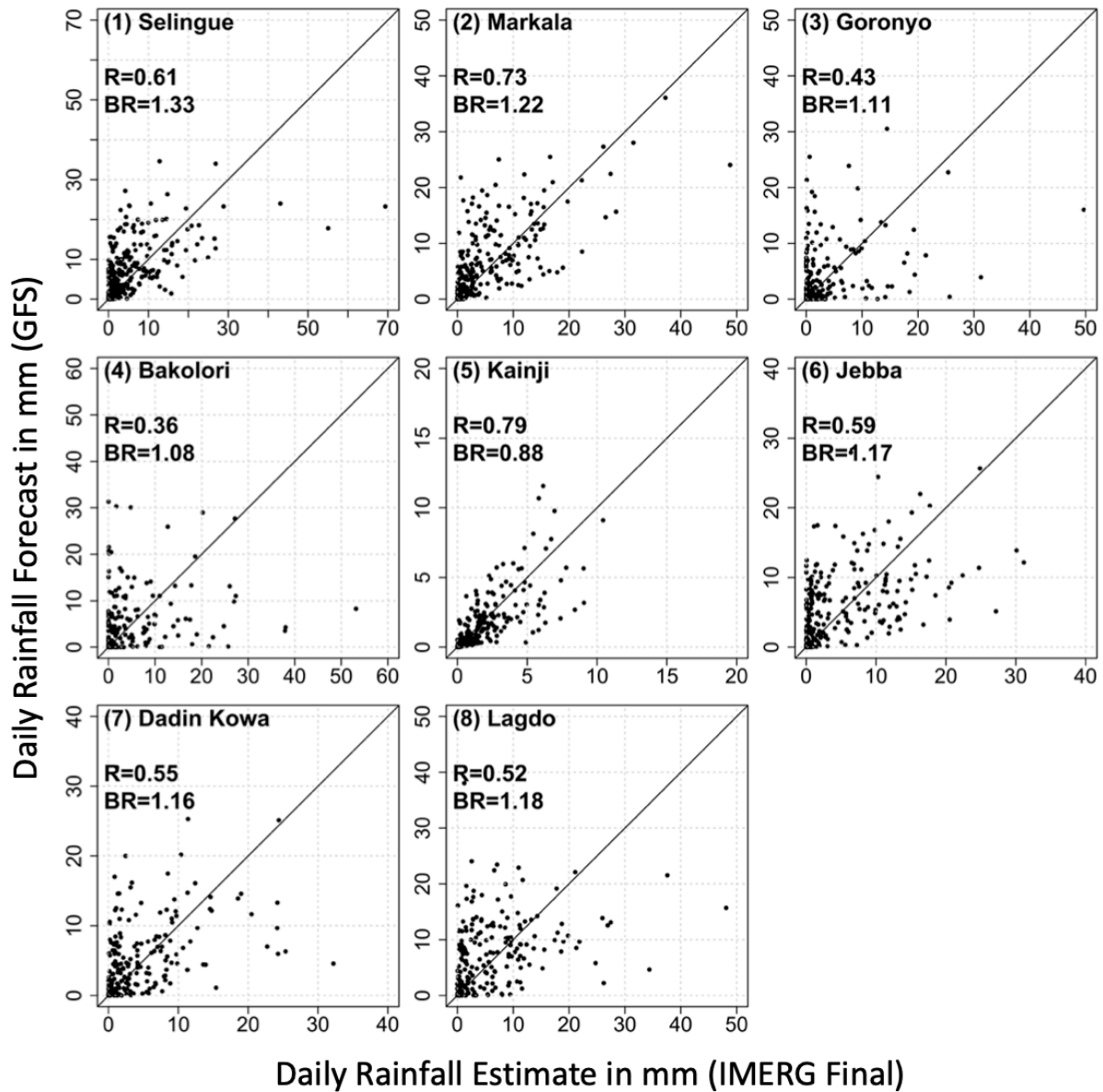
Figure 8. Scatterplot of watershed-averaged daily precipitation forecast obtained from 1-day lead GFS forecasts against corresponding values from IMERG Final.

358

359

3.5 Dependence of Daily Forecast Performance on Lead Time and Spatial Scale

In order to assess the effect of various lead times and spatial scales on forecast performance, we obtained daily GFS forecasts at various lead times (1-day, 5-day, 10-day, and 15-day), and aggregated the forecasts at spatial scales from 0.25° to coarser scales (0.5°, 0.75°, and 1°) by averaging grids. The purpose of degrading the resolution is to determine at which resolution the forecasts have acceptable performance. The KGE value at each spatial resolution was calculated in the following steps: (i) average the data at the required spatial resolution, (ii) extract pairs of data (one from IMERG Final, and the other from GFS), (iii) concatenate the pairs to form one large series of data, and (4) compute a single KGE from this data series. The resulting KGE values are shown in Fig. 9.

With regard to the effect of spatial scales, the KGE at the GFS native resolution (i.e. 0.25°) is very low. As the spatial scale increases, KGE increases, as expected. For instance, for Markala watershed KGE increases from 0.27 (0.25°) to 0.40 (1°) for a 1-day lead. This indicates that the variation in KGE values between the watersheds could be partly explained by the watershed size. For example, based on Fig. 5, the KGE for the 1-day lead daily GFS forecast was the highest for the largest Kainji watershed (watershed area of 1,464,092 Km^2) and the lowest for the smallest Bakolori watershed (4,887 Km^2). With regard to the effect of lead time for daily forecasts, KGE decreases significantly as lead time increases. For instance, for Markala watershed and a grid size of 1°, KGE decreases from 0.40 (1-day lead) to 0.21 (15-day lead).

379
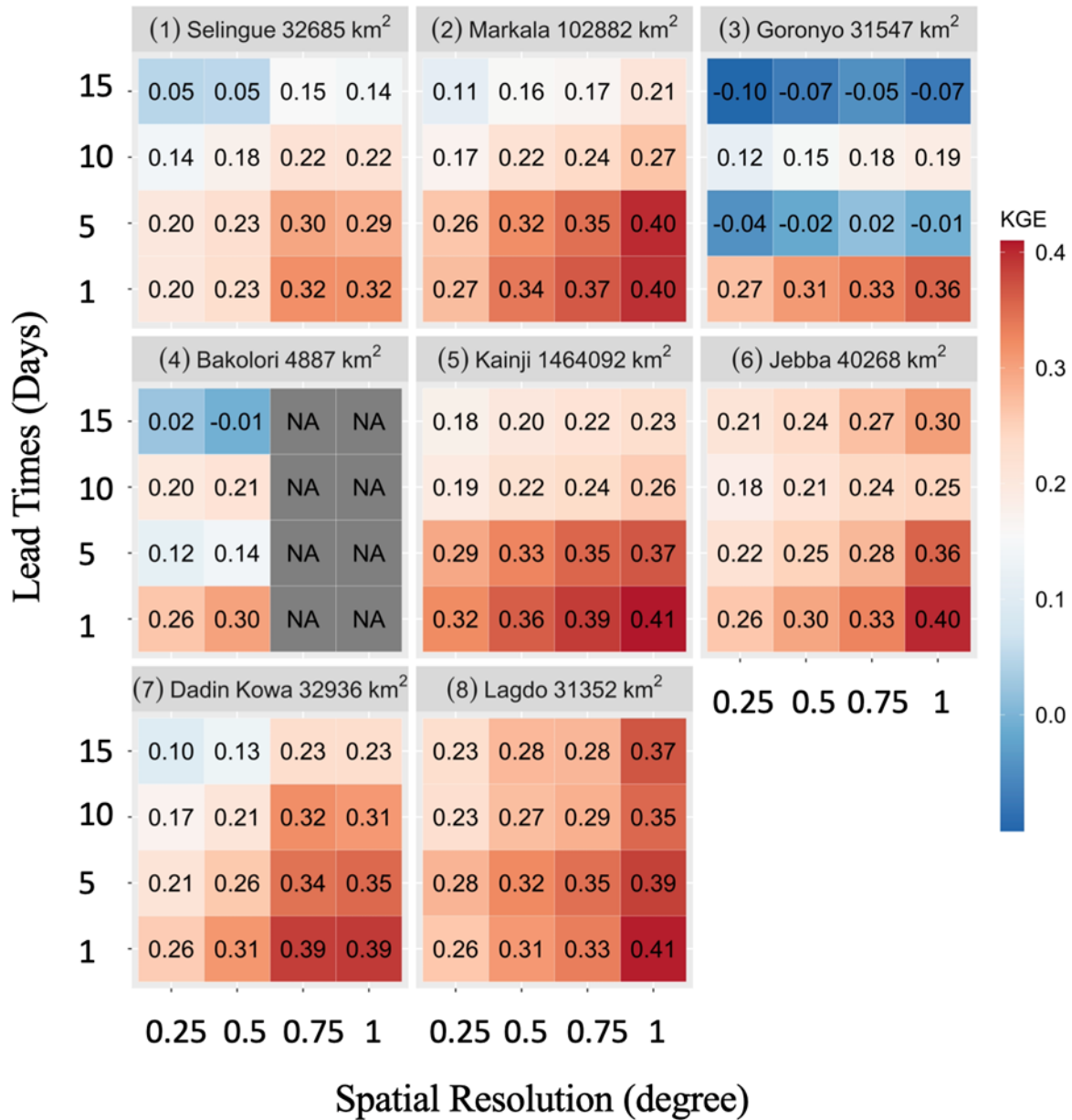
380
381 Figure 9. Kling-Gupta Efficiency (KGE) for daily precipitation of GFS as a function of lead time (1-day, 5-day, 10-
382 day, and 15-day) and spatial scale (0.25°, 0.50°, 0.75°, 1.0°). The dam names and corresponding watershed areas are
383 given in the titles.
384

385 **3.6 Effect of Temporal Aggregation Scale on Forecast Performance**

386 To assess the effect of temporal aggregation scale, we obtained the 1-day total, 5-day total, 10-day total, and 15-day

387 total GFS precipitation forecasts. These multi-day forecasts are constructed by combining multiple lead-time forecasts.

388 For instance, the 5-day total forecast is obtained by adding the 1-day lead, 2-day lead, 3-day lead, 4-day lead, and 5-

389   day lead daily forecasts. Figure 10 presents the KGE values for GFS forecasts over different temporal aggregation

390   scales, and different grid sizes. Temporal aggregation substantially increases KGE at all spatial scales. For example,

391   at the grid size of 1° over Markala watershed, the KGE values jump from 0.40 at daily timescale to 0.73 at 15-day

392   total timescale.
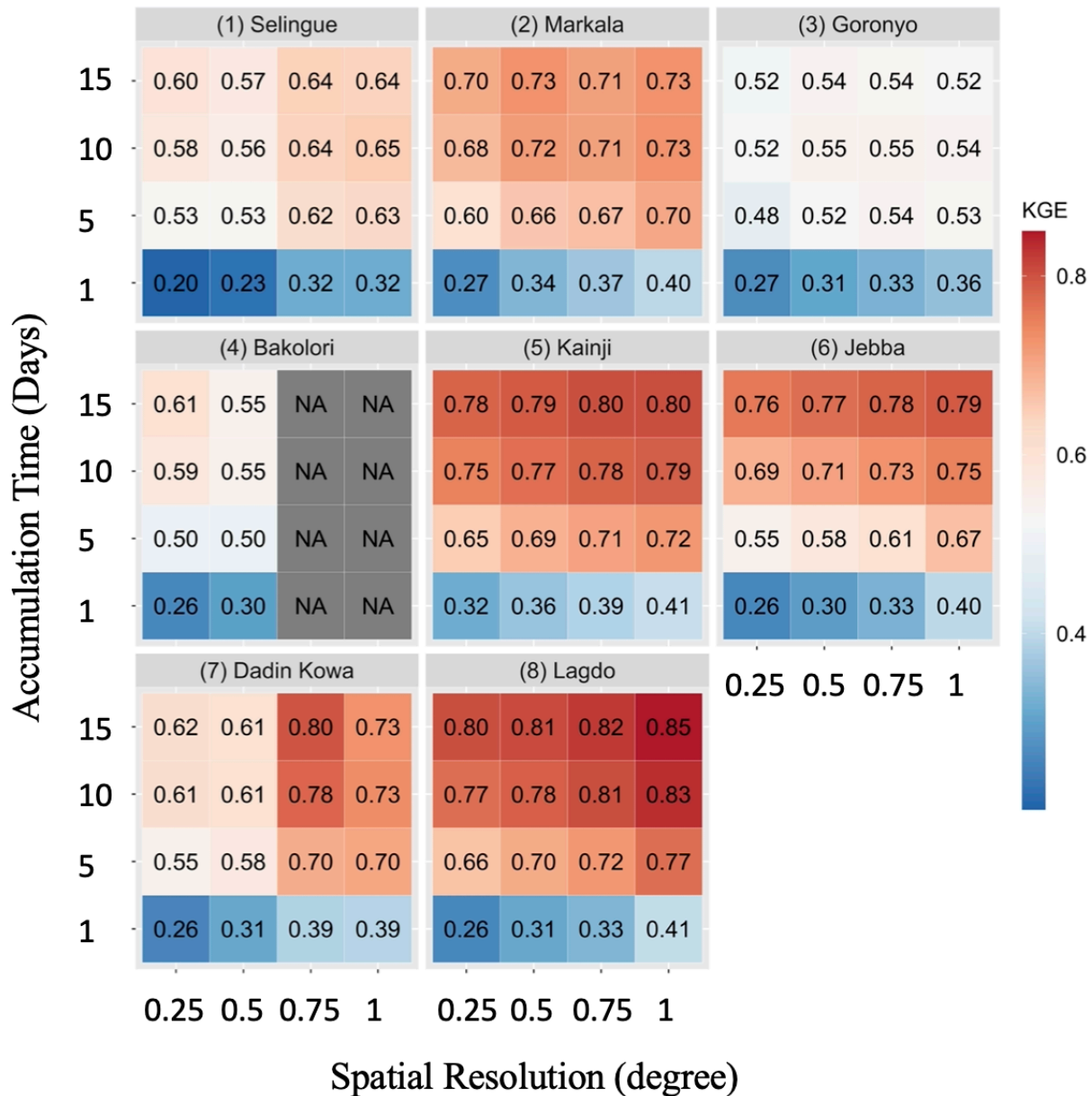
393   Figure 10. Kling-Gupta Efficiency (KGE) of GFS as a function of accumulation time scale (1-day, 5-day, 10-day,
394   and 15-day) and spatial scale (0.25°, 0.50°, 0.75°, 1.0°).
395

396   In Figure 11, we show the performance statistics of GFS for 15-day accumulated watershed-averaged rainfall forecast.

397   The KGE values are intermediate (0.5 < KGE < 0.75) for four watersheds and good (KGE > 0.75) for the remaining

398   four watersheds. Analysis of the components of KGE reveals that the improvement of KGE at longer timescales comes

399   as a result of improved correlation and variability ratio. At the 15-day accumulation timescale, IMERG Early estimates

400   have less bias than GFS at all watersheds, except at Kainji watershed. Figure 12 presents the scatterplot of 15-day

401   accumulated GFS forecast vs IMERG Final. In general, the GFS estimates perform well for low to moderate rain rates,

402   but tend to overestimate higher rain rates. This is consistent with Wang et al. (2019) who reported the difficulty of

403   capturing the magnitude of high rain rates in GFS model.
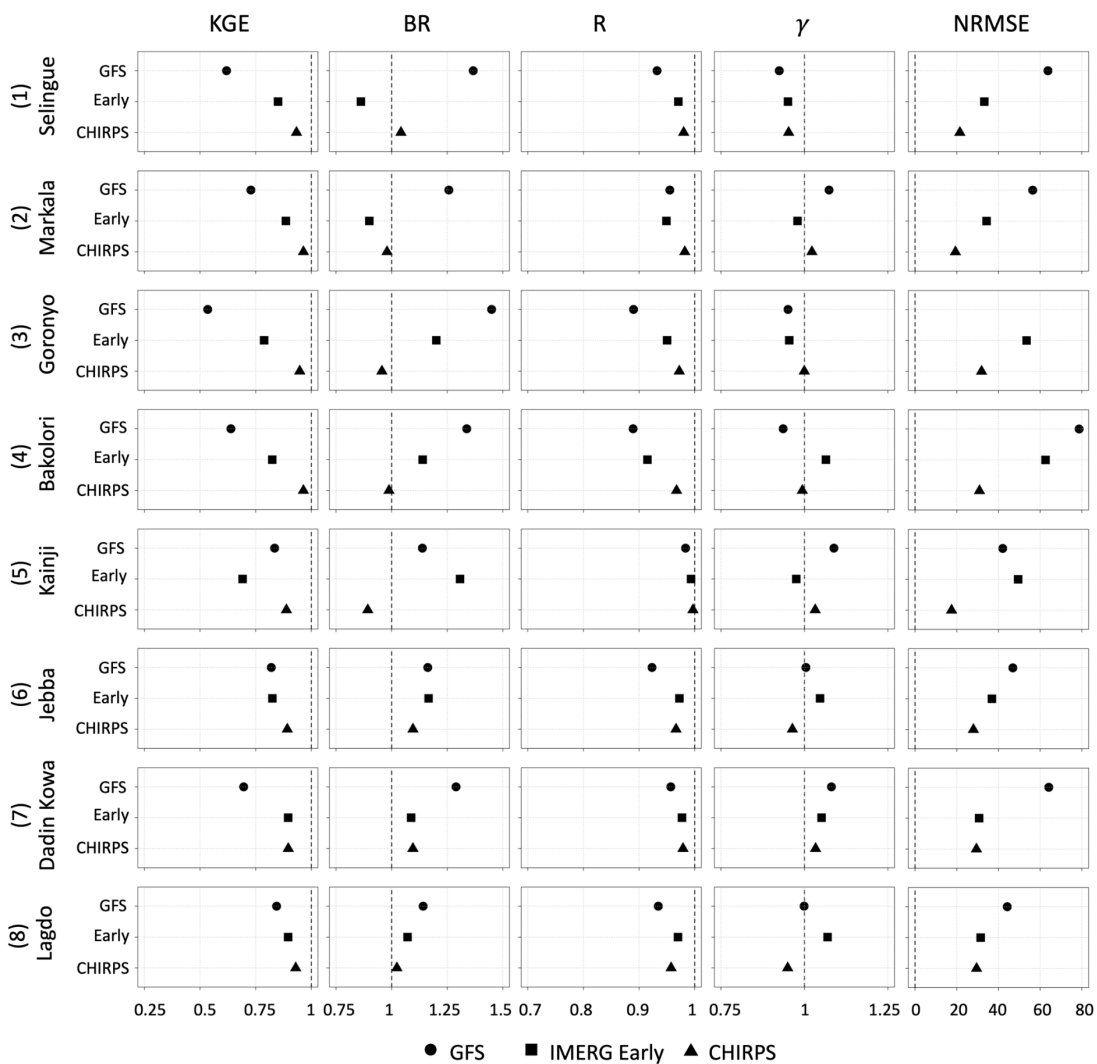
404   Figure 11. Summary of performance statistics (Kling-Gupta Efficiency KGE, Bias Ratio BR, correlation R,
405   variability ratio γ, and root mean square error normalized by reference rainfall [%], for the 15-day accumulated GFS
406   forecast and other satellite products.
407
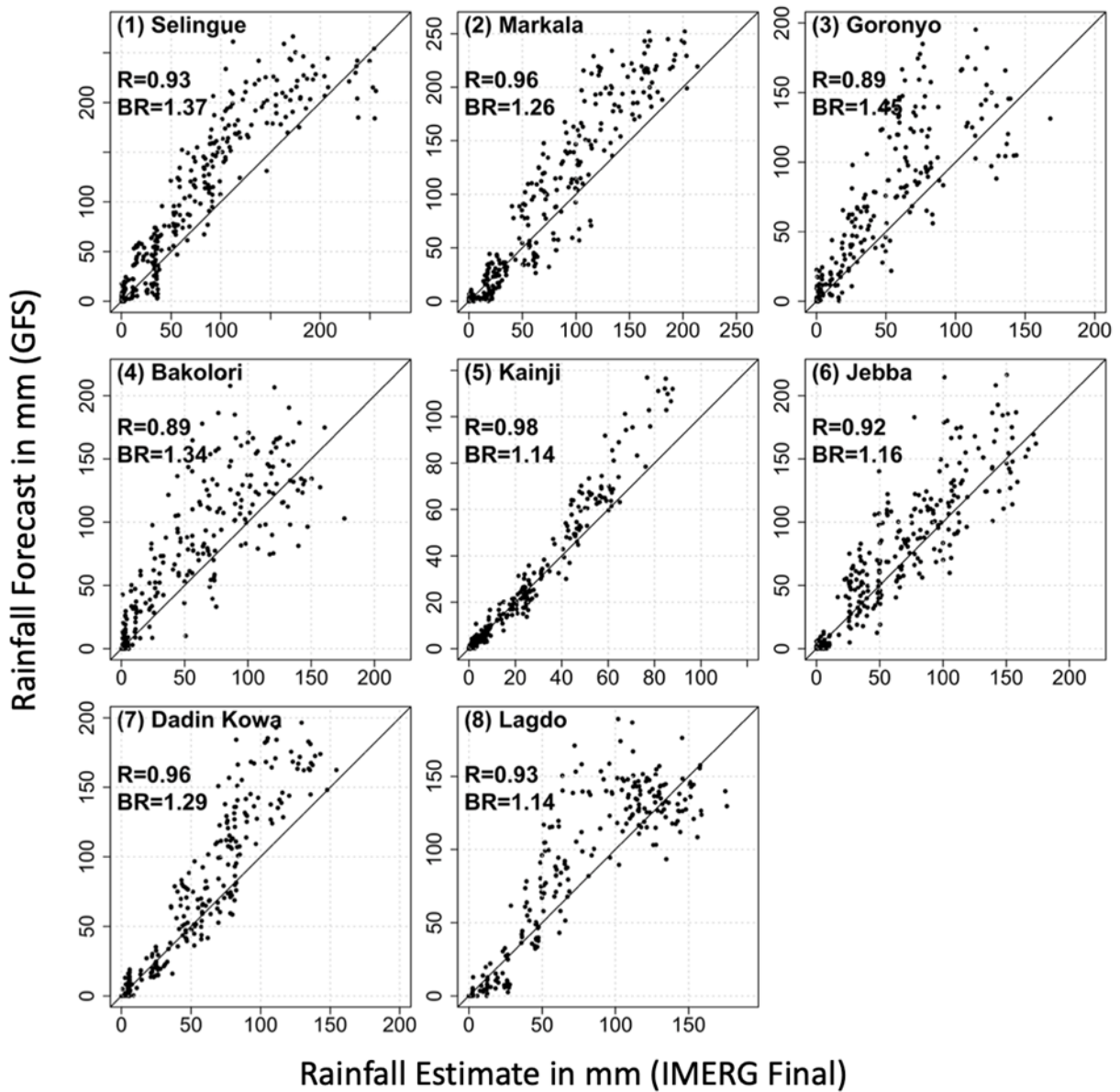
Figure 12. Scatterplot of watershed-averaged 15-day accumulated precipitation forecast obtained from GFS forecast against corresponding values from IMERG Final.

4. Conclusions

This study has evaluated the accuracy of medium-range (1-day to 15-day lead time) forecasts available from the Global Forecast System (GFS), for the watersheds of large dams in the Niger river basin. Despite the limited temporal coverage, some consistent features emerged from this evaluation. The accuracy of GFS forecast depends on climatic regime, lead time, accumulation timescale, and spatial scale. With regard to the role of climatic regimes, the GFS

forecast has large overestimation bias in the Guinea (wet climatic regime), moderate overestimation bias in the Savannah (moderately wet climatic regime), but has no bias in the Sahel (dry climate). With regard to lead time, as the lead time increases, the forecast accuracy decreases. Averaging the forecasts at coarser spatial scales leads to increased forecast accuracy. For daily rainfall forecasts, the performance of GFS is very low (KGE < 0.32) at almost all watersheds except at Markala (KGE = 0.44) and Kainji (KGE = 0.68), both of which have much larger watershed areas compared to the other watersheds. Averaging the forecasts at longer time scales also leads to increased forecast accuracy. For 15-day rainfall accumulation timescale, the KGE values are either "intermediate" (i.e., $0.50 \leq KGE \leq 0.75$) for half of the watersheds (Selingue, Goronyo, Bakolori, and Daddin Kowa) or "good" (i.e., KGE ≥ 0.75) for the remaining half (Markaa, Kainji, Jebba, and Lagdo). With regard to the effect of rainfall rate, the 15-day accumulated GFS forecasts tend to perform better for low to medium rain rates, but contain large overestimation bias at high rain rates.

The performance statistics of GFS indicate the need for calibrating GFS forecasts in order to improve their accuracy. Post-processing calibration of GFS forecasts requires the use of "relatively better performing" and "available in near-real-time" independent rainfall observations to correct real-time dynamical GFS model forecasts. This study has compared the performance of IMERG Early satellite rainfall products with the performance of GFS in terms of bias. In the Guinea and Savannah regions, IMERG Early outperforms GFS in terms of bias, while in the dry Sahel region, IMERG Early is outperformed by GFS.

We acknowledge that the reference dataset used in our evaluation (i.e., IMERG Final) has its own estimation errors. We conducted additional assessment to evaluate the performance of IMERG Final with respect to another independent and high-quality (i.e. satellite-gauge merged) rainfall product (i.e. CHIRPS). Our results show that IMERG Final and CHIRPS have similar rainfall characteristics, indicating the robustness of IMERG Final.

Overall, we conclude that the GFS forecasts, at 15-day accumulation timescale, have acceptable performance, although they tend to overestimate high rain rates. The shorter the time scale, the lower is the GFS performance. We recommend identifying suitable post-processing calibration techniques, through the use of near-real time products, such as, IMERG Early, that could improve the performance of GFS, particularly in the wet Guinea and Savannah

regions. Possible calibration methods that could be explored include: simple bias (multiplicative) correction, multi-resolution bias correction through wavelet analysis wavelet analysis or empirical mode decomposition method, and Artificial-based methods such as Feed Forward Neural Network (FFNN), Support Vector Machine (SVR), and Adaptive Neural Fuzzy Inference System (ANFIS).

5. Data and Code Availability

We acknowledge the National Center for Atmospheric Research (NCAR) for providing public access to the GFS rainfall forecast data products (https://rda.ucar.edu/datasets/ds084.1/), NASA for providing public access to IMERG Final and IMERG Early rainfall data products (https://disc.gsfc.nasa.gov), and the University of California Santa Barbara's (UCSB) Climate Hazard's group for providing public access to CHIRPS rainfall data (https://www.chc.ucsb.edu/data).

6. Author Contribution

H. Yue: data processing, data analysis, and manuscript preparation; M. Gebremichael: project oversight, method design, contribution to manuscript text; V. Nourani: method design, contribution to manuscript text.

7. Competing Interests

The authors declare that they have no conflict of interest.

8. Acknowledgement

We acknowledge funding support from NASA Precipitation Measurement Mission through Grant # 80NSSC19K0688.

493 **References**

494 Abdalla, S., Janssen, P. A., Balmaseda, M. A., Mogensen, K., Bidlot, J. R., & Keeley, S.: ECMWF Experience In
495 Global Monitoring And Validation Of Radar Altimetry Products. In ESA Living Planet Symposium 2013, 9-13 Sep.
496 2013, Edinburgh, ESA Proceedings No. SP-722 (CD), 2013 December

497 Akinsanola, A. A., and Zhou, W.: Projections of West African summer monsoon rainfall extremes from two CORDEX
498 models. Climate Dynamics, 52(3), 2017-2028, doi:10.1007/s00382-018-4238-8, 2018

499 Akinsanola, A. A., Ogunjobi, K. O., Gbode, I. E., and Ajayi, V. O.: Assessing the capabilities of three regional climate
500 models over CORDEX Africa in simulating West African summer monsoon precipitation. Advances in Meteorology,
501 doi:10.1155/2015/935431, 2015.

502 Akinsanola, A.A., Ajayi, V.O., Adejare, A.T., Adeyeri, O.E., Gbode, I.E., Ogunjobi, K.O., Nikulin, G. and Abolude,
503 A.T.: Evaluation of rainfall simulations over West Africa in dynamically downscaled CMIP5 global circulation
504 models. Theoretical and applied climatology., 132(1), 437-450, doi:10.1007/s00704-017-2087-8, 2017.

505 Alexander, S., Yang, G., Addisu, G., and Block, P.: Forecast-informed reservoir operations to guide hydropower and
506 agriculture allocations in the Blue Nile basin, Ethiopia. International Journal of Water Resources Development, 1-26,
507 doi:10.1080/07900627.2020.1745159, 2020

508 Alfieri, L., Burek, P., Dutra, E., Krzeminski, B., Muraro, D., Thielen, J., and Pappenberger, F.: GloFAS–global
509 ensemble streamflow forecasting and flood early warning. Hydrology and Earth System Sciences, 17(3), 1161-1175,
510 doi:10.5194/hess-17-1161-2013, 2013

511 Animashaun, I. M., Oguntunde, P. G., Akinwumiju, A. S., and Olubanjo, O. O.: Rainfall Analysis over the Niger
512 Central Hydrological Area, Nigeria: Variability, Trend, and Change point detection. Scientific African, 8, e00419,
513 doi: 10.1016/j.sciaf.2020.e00419, 2020

514 Arakawa, A., and Schubert, W. H.: Interaction of a cumulus cloud ensemble with the large-scale environment, Part I.
515 Journal of the Atmospheric Sciences, 31(3), 674-701, 1974.

516 Bhuiyan, M.A., Nikolopoulos. E.I., and Anagnostou, E.N.: Machine Learning-Based Blending of Satellite and
517 Reanalysis Precipitation Datasets: A Multiregional Tropical Complex Terrain Evaluation, Journal of
518 Hydrometeorology, 20(11), 2147-2161, doi: 10.1175/JHM-D-19-0073.1, 2019.

519 Bliefernicht, J., Waongo, M., Salack, S., Seidel, J., Laux, P., and Kunstmann, H.: Quality and value of seasonal
520 precipitation forecasts issued by the West African regional climate outlook forum. Journal of Applied Meteorology
521 and Climatology, 58(3), 621-642, doi:10.1175/JAMC-D-18-0066.1, 2019.

522 Breuer, N. E., Fraisse, C.W., and Cabrera, V.E.: The Cooperative Extension Service as a boundary organization for
523 diffusion of climate forecasts: A 5-year study. Journal of Extension, 48(4), 2010, Article Number 4RIB7, 5 pp.

524 Chen, F., Janjić, Z., and Mitchell, K. Impact of atmospheric surface-layer parameterizations in the new land-surface
525 scheme of the NCEP mesoscale Eta model. Boundary-Layer Meteorology, 85(3), 391-421, doi:
526 10.1023/A:1000531001463, 1997.

527 Clough, S., Shephard, M., Mlawer, E., Delamere, J., Iacono, M., Cady-Pereira, K., Boukabara, S., and Brown, P.:
528 Atmospheric radiative transfer MODELING: A summary of the AER codes. Journal of Quantitative Spectroscopy
529 and Radiative Transfer, 91(2), 233-244. doi:10.1016/j.jqsrt.2004.05.058, 2005.

530 Dembélé, M., Schaefli, B., van de Giesen, N., and Mariéthoz, G.: Suitability of 17 rainfall and temperature gridded
531 datasets for largescale hydrological modelling in West Africa. Hydrol. Earth Syst. Sci. Discuss., https://doi.
532 org/10.5194/hess-2020-68, in review, 2020

533 Dezfuli, A. K., Ichoku, C. M., Huffman, G. J., Mohr, K. I., Selker, J. S., Van De Giesen, N., Hochreutener, R., and
534 Annor, F. O.: Validation of IMERG precipitation in Africa. Journal of hydrometeorology, 18(10), 2817-2825, doi:
535 10.1175/JHM-D-17-0139.1, 2017a

536 Dezfuli, A. K., Ichoku, C. M., Mohr, K. I., & Huffman, G. J.: Precipitation characteristics in West and East Africa
537 from satellite and in situ observations. Journal of Hydrometeorology, 18(6), 1799-1805, doi:10.1175/JHM-D-17-
538 0068.1, 2017b

Funk, C., Peterson, P., Landsfeld, M., Pedreros, D., Verdin, J., Shukla, S., Husak, G., Rowland, J., Harrison, L., Hoell, A., and Michaelsen, J.: The climate hazards infrared precipitation with stations—a new environmental record for monitoring extremes. Scientific data, 2(1), 1-21, doi:10.1038/sdata.2015.66, 2015.

Gossett, M., Alcoba, M., Roca, R., Cloche, S., and Urbani, G.: Evaluation of TAPEER daily estimates and other GPM-era products against dense gauge networks in West Africa, analysing ground reference uncertainty. 144(1), 255-269, doi: 10.1002/qj.3335, 2018.

Grell, G. A.: Prognostic evaluation of assumptions used by cumulus parameterizations. Monthly weather review, 121(3), 764-787, doi: 10.1175/1520-0493(1993)121<0764:PEOAUB>2.0.CO;2, 1993.

Gupta, H. V., Kling, H., Yilmaz, K. K., and Martinez, G. F.: Decomposition of the mean squared error and NSE performance criteria: Implications for improving hydrological modelling. Journal of hydrology, 377(1-2), 80-91, doi: 10.1016/j.jhydrol.2009.08.003, 2009.

Haile, A. T., Tefera, F. T., and Rientjes, T.: Flood forecasting in Niger-Benue basin using satellite and quantitative precipitation forecast data. International journal of applied earth observation and geoinformation, 52, 475-484, doi: 10.1016/j.jag.2016.06.021, 2016.

Hou, A. Y., Kakar, R. K., Neeck, S., Azarbarzin, A. A., Kummerow, C. D., Kojima, M., Oki, R., Nakamura, K., and Iguchi, T.: The global precipitation measurement mission. Bulletin of the American Meteorological Society, 95(5), 701-722, doi:10.1175/BAMS-D-13-00164.1, 2014.

Huffman, G. J., Adler, R., Bolvin, D., and E. Nelkin, E.: The TRMM Multi-Satellite Precipitation Analysis (TMPA). Satellite Rainfall Applications for Surface Hydrology, M. Gebremichael and F. Hossain, Eds., Springer, 3–22, 2010.

Huffman, G. J., Bolvin, D. T., Braithwaite, D., Hsu, K., Joyce, R., Xie, P., & Yoo, S. H.: NASA global precipitation measurement (GPM) integrated multi-satellite retrievals for GPM (IMERG). Algorithm Theoretical Basis Document (ATBD) Version, 4, 26, 2015.

Huffman, G. J., Bolvin, D. T., Nelkin, E. J., Wolff, D. B., Adler, R. F., Gu, G., Hong, Y., Bowman, K.P. and Stocker, E. F.: The TRMM Multisatellite Precipitation Analysis (TMPA): Quasi-Global, Multiyear, Combined-Sensor Precipitation estimates at fine scales. Journal of Hydrometeorology, 8(1), 38-55. doi:10.1175/jhm560.1, 2007.

Huffman, G.J., Stocker, E.F., Bolvin, D.T., Nelkin, E.J., Jackson J.: GPM IMERG Final Precipitation L3 1 day 0.1 degree x 0.1 degree V06, Edited by Andrey Savtchenko, Greenbelt, MD, Goddard Earth Sciences Data and Information Services Center (GES DISC), Accessed: [Feb 11, 2021], doi:10.5067/GPM/IMERGDF/DAY/06, 2019a

Huffman, G.J., Stocker, E.F., Bolvin, D.T., Nelkin, E.J., Jackson J.: GPM IMERG Early Precipitation L3 1 day 0.1 degree x 0.1 degree V06, Edited by Andrey Savtchenko, Greenbelt, MD, Goddard Earth Sciences Data and Information Services Center (GES DISC), Accessed: [Feb 11, 2021], doi:10.5067/GPM/IMERGDE/DAY/06, 2019b

Iacono, M. J., Mlawer, E. J., Clough, S. A., and Morcrette, J. J.: Impact of an improved longwave radiation model, RRTM, on the energy budget and thermodynamic properties of the NCAR community climate model, CCM3. Journal of Geophysical Research: Atmospheres, 105(D11), 14873-14890, doi: 10.1029/2000JD900091, 2000.

Jiang, M., Feng, J., Li, Z., Sun, R., Hou, Y. T., Zhu, Y., Wan, B., Guo, J., and Cribb, M.: Potential influences of neglecting aerosol effects on the NCEP GFS precipitation forecast. Atmospheric Chemistry and Physics, 17(22), 13967–13982, doi: 10.5194/acp-17-13967-2017, 2017.

JMA.: Outline of the operational numerical weather prediction at the Japan Meteorological Agency (Appendix to WMO numerical weather prediction progress report). Japan Meteorological Agency, 47pp. (available online at https://www.jma.go.jp/jma/jma-eng/jma-center/nwp/outline2019-nwp/index.htm; last accessed: February 2021), 2019.

Kling, H., Fuchs, M., and Paulin, M.: Runoff conditions in the upper Danube basin under an ensemble of climate change scenarios. Journal of Hydrology, 424, 264-277, 2012.

Koppa, A., Gebremichael, M., Zambon, R.C., Yeh, W.W.G., and Hopson, T.M.: Seasonal Hydropower Planning for Data-Scarce Regions Using Multimodel Ensemble Forecasts, Remote Sensing Data, and Stochastic Programming. WATER RESOURCES RESEARCH, 55(11), 8583-8607, DOI: 10.1029/2019WR025228, 2019.

586 Lehner, B., and 14 coauthors: High-resolution mapping of the world's reservoirs and dams for sustainable river-flow
587 management. Frontiers in Ecology and the Environment 9 (9): 494-502, 2011

588 Lehner, B., Verdin, K., Jarvis, A.: New global hydrography derived from spaceborne elevation data. Eos, Transactions,
589 AGU, 89(10): 93-94, 2008

590 Lien, G. Y., Kalnay, E., Miyoshi, T., and Huffman, G. J.: Statistical properties of global precipitation in the NCEP
591 GFS model and TMPA observations for data assimilation. Monthly Weather Review, 144(2), 663–679, doi:
592 10.1175/MWR-D-15-0150.1, 2016.

593 Maranan, M., Fink, A. H., Knippertz, P., Amekudzi, L. K., Atiah, W. A., and Stengel, M.: A process-based validation
594 of GPM IMERG and its sources using a mesoscale rain gauge network in the West African forest zone. Journal of
595 Hydrometeorology, 21(4), 729-749, 2020

596 Mase, A. S., and Prokopy, L.S.: Unrealized Potential: A review of perceptions and use of weather and climate infor-
597 mation in agricultural decision making. Weather Climate and Society 6(1):47-61. DOI: 10.1175/Wcas-D-12-00062.1,
598 2014.

599 Mlawer, E. J., Taubman, S. J., Brown, P. D., Iacono, M. J., and Clough, S. A.: Radiative transfer for inhomogeneous
600 atmospheres: RRTM, a validated correlated-k model for the longwave. Journal of Geophysical Research:
601 Atmospheres, 102(D14), 16663-16682, 1997.

602 National Centers for Environmental Prediction.: National Centers for Environmental Prediction: The Global Forecast
603 System   (GFS)   -Global   Spectral   Model   (GSM).   Retrieved   from
604 https://www.emc.ncep.noaa.gov/emc/pages/numerical_forecast_systems/gfs/documentation.php, last access: Sep
605 2021, 2021a

606 National Centers for Environmental Prediction.: National Centers for Environmental Prediction: FV3: The GFDL
607 Finite-Volume Cubed-Sphere Dynamical Core, Retrieved from https://www.gfdl.noaa.gov/fv3/, last access: Sep 2021,
608 2021b

609 National Centers for Environmental Prediction/National Weather Service/NOAA/U.S. Department of Commerce.:
610 NCEP GFS 0.25 Degree Global Forecast Grids Historical Archive, doi:10.5065/D65D8PW, 2015

611 Pandya, R., Hodgson, A., Hayden, M.H., Akweongo, P., Hopson, T., Forgor, A.A., Yoksas, T., Dalaba, M.A., Dukic,
612 V., Mera, R., and Dumont, A., McCormack, K., Anaseba, D., Awine, T., Boehnert, J., Nyaaba, G., Laing, A., and
613 Semazzi, F.: Using weather forecasts to help manage meningitis in the West African Sahel. Bulletin of the American
614 Meteorological Society 96(1):103-+. doi: 10.1175/Bams-D-13-00121.1, 2015

615 Patt, A. G., Ogallo, L., and Hellmuth, M.: Sustainability—Learning from 10 years of climate outlook forums in Africa.
616 Science 318(5847):49-50. doi:10.1126/science.1147909, 2007.

617 Pirret, J. S., Daron, J. D., Bett, P. E., Fournier, N., and Foamouhoue, A. K.: Assessing the skill and reliability of
618 seasonal climate forecasts in Sahelian West Africa. Weather and Forecasting, 35(3), 1035-1050, doi:10.1175/WAF-
619 D-19-0168.1, 2020.

620 Roudier, P., Alhassane, A., Baron, C., Louvet, S., and Sultan, B.: Assessing the benefits of weather and seasonal
621 forecasts to millet growers in Niger. Agricultural and forest meteorology, 223, 168-180, doi:
622 10.1016/j.agrformet.2016.04.010, 2016.

623 Saha, S., Moorthi, S., Wu, X., Wang, J., Nadiga, S., Tripp, P., Behringer, D., Hou, Y.-T., Chuang, H.-Y., Iredell, M.,
624 Ek, M., Meng, J., Yang, R., Mendez, M.P., van den Dool, H., Zhang, Q., Wang, W., Chen, M., and Becker, E.: The
625 NCEP climate forecast system version 2. Journal of climate, 27(6), 2185-2208, doi:10.1175/JCLI-D-12-00823.1,
626 2014.

627 Satgé, F., Defrance, D., Sultan, B., Bonnet, M. P., Seyler, F., Rouché, N., and Paturel, J. E.: Evaluation of 23 gridded
628 precipitation datasets across West Africa. Journal of Hydrology, 581, 124412, doi:10.1016/j.jhydrol.2019.124412 ,
629 2020.

630 Sorí, R., Nieto, R., Drumond, A., and Gimeno, L.: The Niger River Basin Moisture Sources: A Lagrangian
631 Analysis. Atmosphere, 8(2), 38, doi: 10.3390/atmos8020038, 2017.

Sridevi, C., Singh, K. K., Suneetha, P., Durai, V. R., and Kumar, A.: Rainfall forecast skill of Global Forecasting System (GFS) model over India during summer monsoon 2015. Geofizika, 35(1), 39–52, doi: 10.15233/gfz.2018.35.4, 2018.

Sylla, M. B., Faye, A., Giorgi, F., Diedhiou, A., and Kunstmann, H.: Projected heat stress under 1.5 C and 2 C global warming scenarios creates unprecedented discomfort for humans in West Africa. Earth's Future, 6(7), 1029-1044, doi: 10.1029/2018EF000873, 2018.

Tian, D., Wood, E.F., and Yuan, X.: CFSv2-based sub-seasonal precipitation and temperature forecast skill over the contiguous United States. Hydrology and Earth System Sciences, 21, 1477–1490, doi:10.5194/hess-21-1477-2017, 2017.

Towner, J., Cloke, H.I., Zsoter, E., Flamig, Z., Hoch, J.M., Bazo, J., de Perez, E.C., and Stephens, E.M.: Assessing the performance of global hydrological models for capturing peak river flows in the Amazon basin. Hydrology and Earth System Sciences, 23, 3057–3080, doi:10.5194/hess-23-3057-2019, 2019.

van de Giesen, N., Hut, R., & Selker, J.: The trans-African hydro-meteorological observatory (TAHMO). Wiley Interdisciplinary Reviews: Water, 1(4), 341-348, doi:10.1002/wat2.1034, 2014

Wang, J. W. A., Sardeshmukh, P. D., Compo, G. P., Whitaker, J. S., Slivinski, L. C., McColl, C. M., and Pegion, P. J.: Sensitivities of the NCEP global forecast system. Monthly Weather Review, 147(4), 1237–1256, doi: 10.1175/MWR-D-18-0239.1, 2019.

Yuan, X., E. F. Wood, and M. Liang: Integrating weather and climate prediction: toward seamless hydrologic forecasting. Geophysical Research Letters, 41, 5891–5896, doi:10.1002/2014GL061076, 2914.

Zhang, C., Xue, M., Supinie, T. A., Kong, F., Snook, N., Thomas, K. W., Brewster, K., Jung, Y., Harris, L.M. and Lin, S. J.: How well does an FV3-based model predict precipitation at a convection-allowing resolution? Results from CAPS forecasts for the 2018 NOAA hazardous weather test bed with different physics combinations. Geophysical Research Letters, 46(6), 3523-3531, doi:10.1029/2018GL081702, 2019.